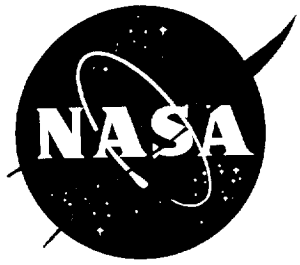

Langley Research Center

Measurement of Separated Flow Structures Using a Multiple-Camera DPIV System

William M. Humphreys, Jr.
Scott M. Bartram
NASA Langley Research Center
Hampton, VA 23681

Presented at the 19th International Congress on Instrumentation in Aerospace Simulation Facilities (ICIASF) 27-30 August 2001 / Cleveland, Ohio

MEASUREMENT OF SEPARATING FLOW STRUCTURES USING A MULTIPLE-CAMERA DPIV SYSTEM

William M. Humphreys, Jr.*
Scott M. Bartram†

NASA Langley Research Center
Hampton, Virginia 23681

ABSTRACT

A novel multiple-camera system for the recording of digital particle image velocimetry (DPIV) images acquired in a two-dimensional separating / reattaching flow is described. The measurements were performed in the NASA Langley Subsonic Basic Research Tunnel as part of an overall series of experiments involving the simultaneous acquisition of dynamic surface pressures and off-body velocities. The DPIV system utilized two frequency-doubled Nd:YAG lasers to generate two coplanar, orthogonally-polarized light sheets directed upstream along the horizontal centerline of the test model. A recording system containing two pairs of matched high resolution, 8-bit cameras was used to separate and capture images of illuminated tracer particles embedded in the flow field. Background image subtraction was used to reduce undesirable flare light emanating from the surface of the model, and custom pixel alignment algorithms were employed to provide accurate registration among the various cameras. Spatial cross correlation analysis with median filter validation was used to determine the instantaneous velocity structure in the separating / reattaching flow region illuminated by the laser light sheets. In operation the DPIV system exhibited a good ability to resolve large-scale separated flow structures with acceptable accuracy over the extended field of view of the cameras. The recording system design provided enhanced performance versus traditional DPIV systems by allowing a variety of standard and non-standard cameras to be easily incorporated into the system.

NOMENCLATURE

d_{camera}	camera pixel spacing, μm
d_{card}	physical spacing of dots on calibration dot card, mm
$\vec{d}$	particle image displacement, uncorrected, μm
$\vec{d}_z$	particle image displacement with zero pulse separation, μm
$\vec{D}$	particle image displacement, corrected, μm, see equation (4)
$f_{kl}(i,j)$	amplitude of i^{th}, j^{th} pixel on camera *l* in receiver *k*
$f'_{kl}(i,j)$	amplitude of background subtracted i^{th}, j^{th} pixel on camera *l* in receiver *k*, see equation (2)
$M_{kl}(i,j)$	amplitude of minimum image i^{th}, j^{th} pixel on camera l in receiver k, see equation (1)
M	magnification of camera system measured from dot card image, see equation (3)
N_p	number of measured pixels between dots on dot card image
$\vec{V}$	particle image / flow velocity, m/sec
$\Delta\tau$	laser pulse separation, μsec
σ_x	standard deviation of parameter X, see equations (5) and (6)

* Research Engineer, Advanced Measurement and Diagnostics Branch
† Engineering Technician, Advanced Measurement and Diagnostics Branch

σ_x^2 variance of parameter X, see equations (5) and (6)

INTRODUCTION

The study of incompressible flow separation and reattachment is classic to fluid dynamics research, and the understanding of such flows is of great importance in many applications. Traditionally these flow structures have been investigated using a variety of probes, surface-mounted sensors, and flow visualization techniques, and an enormous body of data for various model geometries now exists in the literature.[1-2] Historically, most of the data characterizing the global structure of separating flows was of a qualitative nature.[3] However, the development of Particle Image Velocimetry (PIV) in the 1980's followed by Digital Particle Image Velocimetry (DPIV) in the 1990's introduced new techniques for quantitative investigation of complex flow fields. These new techniques have allowed detailed databases to be established, with the work of Grant et.al. presented as one example.[4] PIV is now considered a mature technology for instantaneous planar velocity measurements, and several good review articles appear in the literature which describe the technique in detail.[5-8]

For the past two years the authors, in conjunction with researchers at Michigan State University (MSU), have been conducting simultaneous measurements of dynamic surface pressures and off-body velocities in simplified separating flows. As part of this investigation a series of measurements were conducted using a two-dimensional model tested at low Reynolds number in the NASA Langley Subsonic Basic Research Tunnel (SBRT). The model generated a well-defined separation bubble which was interrogated using a combination of instruments. Dynamic surface pressures were acquired using an 80-element microphone array system while off-body velocities were acquired using a custom DPIV system. An extensive set of data was obtained in SBRT from which new flow measurement techniques and low dimensional models of the flow field are currently being developed.

This paper examines the construction, calibration, and operation of the DPIV system which was employed to collect off-body velocity measurements for the SBRT separated flow characterization studies. In particular, the design of the unique multiple-camera recording system, similar in structure to designs demonstrated by Kahler and Kompenhans,[9] is described in detail. Methods of calibration and relevant error sources associated with the measurements are discussed. Finally, representative data obtained in the facility using the DPIV system is presented.

TUNNEL FACILITY / TEST MODEL

Tunnel Facility

The NASA Langley Subsonic Basic Research Tunnel (SBRT) is an open-circuit wind tunnel containing a rectangular test section measuring 0.84 meters high by 0.57 meters wide by 1.85 meters long. The front portion of the test section contains port and starboard glass windows measuring approximately 0.75- by 0.75 meters, as well as smaller window inserts in the floor and ceiling. The tunnel employs a 6:1 contraction and is capable of a maximum freestream velocity of approximately 60 meters/sec through the use of an axial fan driven by a 200-horsepower variable frequency motor. Tunnel data acquisition hardware includes a 48-channel electronically scanned static pressure monitoring system as well as a series of fixed test section static taps and thermocouples to monitor freestream conditions in real-time. Figure 1 shows a three-dimensional rendered view of the tunnel.

Model

The model employed for this study was designed and built by Laura Hudy in MSU's Department of Mechanical Engineering as part of a NASA Graduate Student Research Program project and consisted of a splitter plate containing a fence attached perpendicularly to the flow at the leading edge.[10] The model was mounted in the center of the SBRT facility such that it bisected the tunnel test section vertically. The model was constructed of aluminum and measured 1.6 meters long by 0.36 meters wide. Aluminum extensions were attached to the model such that the total width of the splitter plate matched the width of the test section. The leading edge fence total height was 34.9 mm, with a step height of 7.9 mm. The fence generated a separated flow region covering approximately 13 percent of the chord length of the splitter plate. This separation zone was maintained as two-dimensional flow

through the use of thin interior side walls attached at the sides of the splitter plate inside the test section – these secondary walls prevented introduction into the separation region of spanwise flow generated by the test section side-wall boundary layers. Flush-mounted glass windows were incorporated into the interior side plates to allow viewing of the centerline flow from outside of the tunnel test section.

The model was populated with an array of 80 flush-mounted, low-cost electret microphones acting as hydrodynamic pressure sensors. The array consisted of 28 microphones mounted along the top centerline of the splitter plate just behind the leading edge fence with two rows each containing 13 microphones located on either side of the centerline. A total of 40 static pressure taps were also located on the top of the splitter plate – 28 taps located parallel to the centerline row of microphones and four other rows each containing 3 taps. A photograph of the model mounted in SBRT showing the dynamic pressure sensors, static taps and interior side wall DPIV windows is given in Figure 2. The acquisition and analysis of the microphone and static tap data is beyond the scope of this paper – reference 10 gives a detailed overview of these topics.

DPIV SYSTEM

The DPIV instrument consisted of five sub-elements, namely a laser optics system, particle seeding system, image recording system, synchronization timing system, and data analysis system. The first four of these sub-elements is described in this section with the data analysis system described subsequently.

Laser Optics

The laser optics system main components included two 600-millijoule, frequency-doubled Nd:YAG pulsed lasers for illumination and a series of optical components for beam combining and light sheet generation. The 532-nm wavelength beams emanating from each laser were aligned to a common optical axis using a half-wave retardation plate and a thin-film polarizing beamsplitter, shown in the schematic of Figure 3. The combined beams were then directed through a series of cylindrical and spherical lenses to generate a long focal length, converging light sheet with minimum thickness of approximately one millimeter and maximum extent of 75 millimeters. The light sheet was directed into the tunnel test section through an access window positioned at the far downstream end of the test section. The sheet was then reflected upstream in the test section along the horizontal centerline of the model and adjusted such that it just grazed the top surface of the splitter plate. This beam path was chosen to minimize flare light reflected from the top surface of the model, allowing measurements to be obtained deeper in the separated flow region boundary layer. Figure 4 shows a photograph of the laser / light sheet system installed in SBRT.

Flow Field Seeding

To provide a uniform distribution of seed in the illuminated region of the flow above the splitter plate, the tunnel was seeded with the chemical bis(2-ethylhexyl) sebacate (commonly known as DEHS). This moderate viscosity, low toxicity oil was injected into the tunnel immediately upstream of the honeycomb section using a six jet atomizer. Figure 5 depicts a typical aerodynamic particle size distribution obtained from atomization of DEHS using a Laskin nozzle, with a mean aerodynamic size of approximately 0.9-1.0 micrometers. It was anticipated that the six jet seeder in SBRT would yield a similar distribution. Control of the seeding density in the tunnel test section was achieved by varying the number of jets operating in the atomizer as well as the pressure delivered to the jets. The seeding delivery system was optimally positioned in front of the tunnel honeycomb section to concentrate the seed in a vertical plane at the center of the tunnel.

Image Recording System

A novel feature of the DPIV system described here concerned the design of the image recording system. To capture illuminated particle images, four matched 1300- by 1030-pixel, 8-bit, progressive scan (full frame) cameras were connected to individual digitizers and frame buffers. The four cameras were arranged in two pairs with each pair forming an independent imaging system (referred to as receivers 1 and 2), each capable of viewing an illuminated planar area measuring 10 cm wide by 8 cm tall at a distance of approximately 1.5 meters. Each camera was attached to a 135-mm, f/2 lens. Receivers 1 and 2 were arranged side by side normal to the light sheet and positioned such that their individual fields of view slightly

overlapped, generating an overall view 19 cm wide by 8 cm tall. Figure 6 contains a photograph showing the recording system installed in the SBRT facility, and Figure 7 shows a photograph of a single receiver with individual components labeled. Note that one of the receivers in Figure 6 is shown mirrored with respect to the other to allow the hardware to be positioned directly adjacent to one another. Nevertheless, the functionality of each receiver was the same.

Data acquisition was achieved for each receiver by means of polarization separation, depicted graphically in Figure 8. Scattered light from particles illuminated within the light sheet were directed to individual cameras in a receiver using a polarizing beamsplitter and flat mirror. The process began by generating a linearly polarized (p-polarization), 10-nanosecond pulsed light sheet at time t. Particles illuminated by the sheet scattered light which was captured by each receiver in the recording system. The scattered light, also p-polarized, passed directly through the beamsplitter to the line of sight camera in each receiver. This was followed by the generation of a second orthogonally polarized (s-polarization), 10-nanosecond pulsed light sheet at time $t+\Delta\tau$, where $\Delta\tau$ represents the laser pulse separation. The s-polarized scattered light emerged from the beamsplitter at right angles to the incident light and was thus directed to the mirrored camera in each receiver. The polarization of the scattered light was preserved due to the size of the particles being of the same magnitude as the wavelength of the laser light. Preservation of polarization and proper alignment of the polarizing beamsplitters made it possible to capture each of the two illuminated particle images on separate cameras, allowing standard spatial cross correlation techniques to be applied to the data.

This camera arrangement was similar to that described by Kahler and Kompenhans for imaging of two spatially-displaced, double-pulsed light sheets in reference 9. However, the operation of the recording system for this study was different in that two coplanar light sheet pulses were captured by the cameras. While the receiver configuration depicted in Figure 8 was more complex than for traditional DPIV systems, it allowed greater flexibility in construction of the camera geometry. The greatest benefit of this design was that it allowed a variety of rugged commodity cameras to be used in the system versus specialized cross correlation cameras. It also allowed hardware commonality to be achieved with related global velocimetry techniques in use at NASA Langley, in particular Doppler Global Velocimetry which utilizes a very similar camera arrangement.[11]

Timing Synchronization

To ensure proper synchronization of cameras and lasers in the DPIV system, the timing circuit shown in Figure 9 was employed. A pulse generator initiated a continuous 10-Hz TTL pulse train which acted as a master sync signal. This pulse train was connected to the laser timing controller which caused the lasers to fire at a continuous 10-Hz pulse repetition rate to maintain energy stability. The master TTL pulse train was also directed to a slave pulse generator configured for external triggering. Inverted and non-inverted TTL outputs from the slave generator were connected to camera and digitizer trigger inputs, respectively. When the external trigger on the slave generator was enabled, each camera and digitizer would begin acquiring images at 10 frames per second until the external trigger was disabled. Custom software was developed to control the acquisition of image data from the four cameras in the recording system, and allowed a slower acquisition rate to be obtained by providing an image "stride"; i.e., unwanted images were simply skipped and not written to disk during an acquisition cycle.

SYSTEM CALIBRATION

Laser Pulse Separation

The laser pulse separation was monitored by placing a fast rise time photodiode along the periphery of the laser optics system. The photodiode was adjusted to respond to secondary reflections of laser light from lenses, windows, etc. The output of the photodiode was attached to a high speed digital oscilloscope which provided a trace showing the relative amplitude of each laser pulse as well as the pulse separation.

Dot Card Recordings

The DPIV recording system described here relied on a process whereby scattered light from particles at two instances of time were captured on separate cameras. While such an arrangement allowed general purpose cameras to be used, it

also greatly increased the complexity of the calibration process. Since DPIV relies on the tracking of particle images from one laser exposure to another to obtain velocity data, alignment errors in the system shown in Figure 7 (i.e., camera misalignment, polarizer skew, etc.) induce direct and sometimes substantial bias errors in these measured velocities. To help reduce these errors, a card containing a uniform series of dots with a horizontal and vertical dot spacing of 5.7 mm was placed in the plane of the light sheet. Figure 10 depicts one of these dot cards. Using white light illumination of the card, a manual alignment was performed by continuously capturing images from all four cameras. Pairs of images representing the data obtained from a particular receiver were subtracted from one another and a difference image displayed in real time on a monitor. Optimal alignment was achieved by causing as many dots as possible in the field of view of each receiver to "disappear". Once optimal alignment was achieved, a sequence of five images of the dot card was captured by each camera. These dot card images were then used in pixel alignment algorithms, described subsequently, to attempt to minimize spatial distortions and ensure accurate pixel alignment between the pairs of cameras constituting each receiver in the recording system.

Zero Displacement Recordings

As a secondary check on the dot card recordings to ensure the highest registration accuracy among all cameras, a series of zero displacement recordings were performed before data acquisition was initiated. This process consisted of setting the laser pulse separation to zero (i.e., firing both Nd:YAG lasers in unison) and seeding the flow while running the tunnel at a nominal speed (typically 10 – 15 m/sec). A series of images were then captured each containing a uniform spatial distribution of seed across the entire field of view of the recording system. The zero laser pulse separation was designed to remove all flow induced motion from the captured images, leaving only receiver mismatch and optical field distortions to account for movement of particle images. The captured images were processed as regular DPIV data. Note that perfect alignment of both cameras in each receiver of the recording system would have revealed a zero velocity vector in all processed interrogation regions. Such a zero velocity field was impossible to achieve in practice, and thus the analysis of the zero displacement recordings quantified bias errors introduced to the DPIV data due to camera misalignment.

IMAGE PROCESSING

Background Removal

It was desired to obtain DPIV velocity data as close to the top surface of the splitter plate as possible, necessitating that unwanted flare light and background noise in acquired images be removed. The authors chose to use a technique described by Kuhn, Kompenhans, and Monnier to perform this background removal.[12] The technique began with the generation of a series of four "minimum" images, one for each camera in the recording system. These minimum images were computed using sequences of DPIV images acquired by the cameras under normal operating conditions (i.e., seeded flow, nominal laser pulse energy and timing, etc.). Letting $f_{kl}(i,j)$ represent the amplitude of a pixel at position (i,j) for an image taken in a sequence by camera l in receiver k, the minimum image $M_{kl}(i,j)$ for the camera was computed via

$$M_{kl}(i,j) = \begin{cases} f_{kl}(i,j) & \text{if } f_{kl}(i,j) < M_{kl}(i,j) \\ M_{kl}(i,j) & \text{otherwise} \end{cases} \quad (1)$$

Note that $M_{kl}(i,j)$ was computed over all pixels and over all images in a camera sequence. The resulting four minimum images, one for each camera, were subtracted on a pixel by pixel basis from each of the individual images in a sequence, i.e.,

$$f'_{kl}(i,j) = f_{kl}(i,j) - M_{kl}(i,j) \quad (2)$$

The modified images were then used in all subsequent processing.

Camera Pixel Alignment

As discussed previously, accurate pixel registration among cameras in each of the recording system receivers was of paramount importance if velocity field bias errors were to be minimized. The pixel alignment algorithm employed for this study utilized sequences of dot card images (Figure 10) acquired during system calibration. There are numerous techniques for pixel alignment which are described in the literature, including geometric back projection

and second order nonlinear fits (reference 5). For this study the authors chose a piecewise bilinear dewarping technique devised for Doppler Global Velocimetry by Meyers et.al. to remove perspective and optical distortions and "straighten" the card images.[13] The technique began by identifying all card dots in the field of view of each camera and computing the centroid location of each dot to subpixel accuracy. Located dots were then grouped into four- sided polygon regions with a dot located at each vertex. Bilinear dewarping was applied to each polygon to square the region. Each pixel in the squared region was then mapped to its corresponding location (a non-integer quantity) in the original image. The value of the pixel was obtained by applying a weighted average obtained from the four adjacent pixels in the mapped location. This technique was applied to both zero displacement and actual data recordings.

Note that this dewarping procedure maps pixels from one spatial domain to another, causing a corresponding change in apparent camera magnification to occur. To measure the new camera magnification the dot card images were dewarped and the pixel to pixel spacing of adjacent dots (with a physical spacing of 5.7 mm on the card) were measured. The average magnification was then easily computed via

$$M = \frac{(N_p)(d_{ccamera})}{d_{card}} \qquad (3)$$

where d_{card} is the measured dot card dot spacing, N_p is the average number of pixels between adjacent dots on the imaged card, and d_{camera} is the physical distance between adjacent pixels in the camera. Measurements of M were taken both horizontally and vertically to check for consistency in the magnification readings. The two values of M for this study were identical at 0.088 since the cameras employed in the recording system contained detectors consisting of square 6.7-micrometer pixels with 100% fill between pixels.

Image Analysis

Spatial cross correlation analysis was performed for all image pairs obtained from receivers 1 and 2 comprising the recording system. The analysis routines were written by the authors and are based on classical DPIV techniques as described by Raffel et.al. in reference 5. The relevant processing parameters employed for the analyses are tabulated in Table 1.

Table 1. DPIV Processing Parameters

Analysis Method	Multiple Frame Cross Correlation
Interrogation Region Size	64 Pixels Square
Interrogation Region Overlap	50 Percent
Correlation Plane Peak Detection	3-point Parabolic Fit
Image Threshold	150

For each interrogation region examined in a pair of acquired images, the fully corrected (i.e., pixel aligned) average particle image displacement vector, $\vec{D}$, was obtained via subtraction of the vector obtained by analysis of the interrogation region in the dewarped zero displacement image, $\vec{d}_z$, from the vector obtained by analysis of the identical interrogation region in the dewarped data image, $\vec{d}$. The velocity vector was subsequently computed using the laser pulse separation. The calculation is represented via

$$\vec{D} = \frac{\vec{d} - \vec{d}_z}{M}, \quad \vec{V} = \frac{\vec{D}}{\Delta\tau} \qquad (4)$$

Given an image size of 1300- by 1030-pixels and the processing parameters in Table 1, a velocity field containing a maximum of 40 horizontal and 32 vertical vectors could be generated from the analysis. In many cases the velocity field was restricted to a subset of the maximum available depending on regions of interest in the flow.

One of the difficulties encountered in measurement of separating and reattaching flows with DPIV concerns the effect on the cross correlation function of high velocity gradients present in interrogation regions bounding areas of high and low speed flow. For instance, the boundary region between a free stream flow and separation bubble is typically more difficult to accurately measure using cross correlation techniques unless gradients are taken into account. For the results presented in this paper, no corrections for gradients were performed. However, the validation of a gradient correction technique implemented by Dr. Ahmed Naguib at MSU is currently being conducted by the authors

and will be incorporated into the analysis of the SBRT dataset in the near future.

Velocity Field Validation

Incorrect velocity vectors introduced to the output data by the cross correlation analyses were identified and removed using magnitude difference algorithms contained in the CleanVec validation system developed by Soloff and Meinhart at the Laboratory for Turbulence and Complex Flow at the University of Illinois – Urbana.[14] No velocity interpolation was performed for this study.

ERROR ANALYSIS / DISCUSSION

A generalized error analysis for the DPIV measurements constituting this study requires that the accuracy of individual particle image displacements obtained from the cross correlation analysis be quantified. This is not an easy task due to the complexity of the correlation algorithm, and the literature contains numerous DPIV uncertainty investigations. Early work concentrated on the identification of spurious vectors within computed velocity fields and on optimization of the instrument to minimize these errors.[15-16] More recently, Huang et.al. and others have provided techniques for minimizing errors in location estimates of correlation plane peaks.[17]

The authors previously derived generalized expressions for measured particle displacement and velocity uncertainties as part of an application of DPIV to an acoustically excited, zero-mean flow.[18] Using a derivation similar to that given in reference 18, it can be shown for the present study via a Taylor series expansion that the precision errors associated with calculation of individual DPIV displacement and velocity vectors can be expressed by

$$\sigma_D^2 \approx (\frac{1}{M})^2\sigma_d^2 + (\frac{1}{M})^2\sigma_{dz}^2 + (\frac{d_z - d}{M^2})^2\sigma_M^2 - 2(\frac{1}{M})^2\sigma_d\sigma_{dz} + 2(\frac{1}{M})(\frac{d_z - d}{M^2})\sigma_d\sigma_M + 2(\frac{1}{M})(\frac{d - d_z}{M^2})\sigma_{dz}\sigma_M \quad (5)$$

$$\sigma_V^2 \approx (\frac{1}{M\Delta\tau})^2\sigma_d^2 + (\frac{1}{M\Delta\tau})^2\sigma_{dz}^2 + (\frac{d_z - d}{M^2\Delta\tau})^2\sigma_M^2 + (\frac{d_z - d}{M\Delta\tau^2})^2\sigma_{\Delta\tau}^2 - 2(\frac{1}{M\Delta\tau})^2\sigma_d\sigma_{dz} + 2(\frac{1}{M\Delta\tau})(\frac{d_z - d}{M^2\Delta\tau})\sigma_d\sigma_M + 2(\frac{1}{M\Delta\tau})(\frac{d - d_z}{M^2\Delta\tau})\sigma_{dz}\sigma_M \quad (6)$$

where the σ terms represent the precision errors of the variables appearing in equation (4). Note that equations (5) and (6) represent only first order approximations to the actual precision errors; nevertheless, they are instructive in terms of computing approximate bounds on the errors expected in this study. To perform the computation , the following mean values and standard deviations were assumed:

Table 2. Precision Error Parameters

Variable	*Mean*	*Standard Deviation*
M	0.088	0.0023
$\Delta\tau$	40 μsec	100 nsec
d	20 - 67 μm (3 – 10 pixel displacement)	0.67 μm (0.1 pixel)
d_z	0 - 13 μm (0 – 2 pixel displacement)	0.67 μm (0.1 pixel)

The standard deviations in Table 2 were chosen based on conservative estimates of expected precision errors in the measurement of each variable. For instance, the standard deviation in the measured displacement, d, and the measured zero pulse separation displacement, d_z, were based on an assumption that the correlation peak could be located to 0.1-pixel accuracy using the 3-point parabolic fit routine used in the analysis. The standard deviation in the measured magnification was based on an assumption that the centroids of dots identified on the dot card could be located to at least ±1-pixel accuracy. Finally, the standard deviation in the pulse separation was based on an assumption that the pulse generators used to control the laser timing had internal jitters no larger than 100 nanoseconds.

Figure 11 shows some expected velocity uncertainties using equation (6) with the parameters shown in Table 2. The uncertainty is plotted as a percentage of the measured velocity, with these velocities computed using equation (4). A family of curves is shown for three

different zero pulse separation displacements. As one would expect, the percent uncertainty increases as the measured velocity decreases since the measured velocity decreases faster than the standard deviation of the measurement. Nevertheless, for the velocity range shown in Figure 11 for reasonable values of d_z, the precision error is of the order of 5% or less.

Note that this analysis addresses *precision* errors only. Predominant *bias* errors are represented by the magnitude of any residual displacements which remain after the dewarped and pixel aligned zero displacement measurements d_z are subtracted from the data via application of equation (4). The full quantization of these residual bias errors is part of an on-going investigation by the authors.

REPRESENTATIVE RESULTS

A total of 32,800 individual image frames (representing 16,400 DPIV data sets) were acquired over four days of testing using the MSU separated flow model in SBRT. The majority of the data was acquired at a freestream velocity of 15 m/sec and a Reynolds number of 8000 based on the total fence height. Figure 12 shows one instantaneous velocity vector field derived from cross correlation analysis of a typical set of image data. The vector field shows reattachment of the separated flow region at approximately 13 percent of the chord length of the splitter plate. The vector fields acquired by the two receivers in the recording system are denoted in the plot. Note that overlapped vectors are not shown in this set of data. The separated flow region is clearly visible in the right half of the vector field, with reattachment occurring midway along the field of view of the downstream receiver.

CONCLUDING REMARKS

A novel multiple-camera system for the recording of digital particle image velocimetry (DPIV) images acquired in a two-dimensional separating / reattaching flow was successfully deployed for the first time at NASA Langley. The recording system contained two pairs of matched high resolution, 8-bit cameras which were used to separate and capture images of illuminated tracer particles embedded in the flow field. The data analysis system employed several custom algorithms which were applied to the acquired data. Background subtraction based on generation of minimum images was performed to reduce undesirable flare light emanating from the surface of the model. Image dewarping and pixel alignment algorithms using information derived from an examination of dot cards placed in the plane of the light sheet were performed to provide accurate pixel registration among the various cameras. Spatial cross correlation analysis with median filter validation was used to determine the instantaneous velocity structure in the separating / reattaching flow region illuminated by the laser light sheet. In operation the DPIV system exhibited a good ability to resolve large-scale separated flow structures with acceptable accuracy over the extended field of view of the recording system. A simple first-order precision error propagation using conservative estimates of the standard deviations derived from camera magnification and laser timing measurements and cross correlation analysis yielded expected velocity precision errors of 5% or less. The authors believe the multiple camera system described in this paper is a good alternative for applications where cross correlation cameras are either not available or are impractical. Further research is required, however, to fully quantify pixel alignment bias errors associated with the use of separate cameras for cross correlation analysis.

ACKNOWLEDGMENTS

The authors gratefully acknowledge the contributions of Dr. Ahmed Naguib and Laura M. Hudy of the Department of Mechanical Engineering at Michigan State University for their design and construction of the model used in this study, and for their numerous suggestions and advice regarding the analysis of the data obtained with the DPIV system.

REFERENCES

1) Cherry, N.J., Hillier, R., and Latour, M., "Unsteady Measurements in a Separated and Reattaching Flow", *Journal of Fluid Mechanics*, Volume 144, pp. 13-46, 1984.
2) Ruderich, R., and Fernholz, H.H., "An Experimental Investigation of a Turbulent Shear Flow with Separation, Reverse Flow, and Reattachment", *Journal of Fluid Mechanics*, Volume 163, pp. 283-322, 1986.
3) Smits, A.J., "A Visual Study of a Separation Bubble", *Proceeding from International Symposium on Flow Visualization*, Bochum, 1980.

4) Grant, I., Owens, E., and Yan, Y., "Particle Image Velocimetry Measurements of the Separated Flow Behind a Rearward Facing Step", *Experiments in Fluids*, Volume 12, pp. 238-244, 1992.
5) Raffel, M., Willert, C., and Kompenhans, J., *Particle Image Velocimetry: A Practical Guide*, Springer-Verlag, New York, 1998.
6) Stanislas, M., Kompenhans, J., and Westerweel, J. (Eds.), *Particle Image Velocimetry: Progress Towards Industrial Application*, Kluwer Academic Publishers, Boston, 2000.
7) Samimy, M., and Wernet, M.P., "Review of Planar Multiple-Component Velocimetry in High-Speed Flows", *AIAA Journal*, Volume 38, Number 4, pp. 553-574, 2000.
8) Westerweel, J., "Fundamentals of Digital Particle Image Velocimetry", *Measurement Science and Technology*, Volume 8, pp. 1379-1392, 1997.
9) Kahler, C.J., Kompenhans, J., "Fundamentals of Multiple Plane Stereo Particle Image Velocimetry", *Experiments in Fluids (Supplement)*, pp. S70-S77, 2000.
10) Hudy, L.M., "Simultaneous Wall-Pressure Array and PIV Measurements in a Separating/Reattaching Flow Region", *Master's Thesis*, Michigan State University, August, 2001.
11) Meyers, J.F., "Development of Doppler Global Velocimetry for Wind Tunnel Testing", *AIAA Paper 94-2582*, 1994.
12) Kuhn, W., Kompenhans, J., Monnier, J.C., "Full Scale PIV Test in an Industrial Facility", *Particle Image Velocimetry: Progress Towards Industrial Application*, Kluwer Academic Publishers, Boston, pp. 91-150, 2000.
13) Meyers, J.F., "Doppler Global Velocimetry - The Next Generation?", *AIAA Paper 92-3897*, 1992.
14) Soloff, S.M., and Meinhart, C.D., *CleanVec: PIV Vector Validation Software, Version 1.13 Build 41*, Released 1999.
15) Keane, R.D., and Adrian, R.J., "Optimization of Particle Image Velocimeters, Part I: Double Pulsed Systems", *Measurement Science and Technology*, Volume 1, pp. 1202-1215, 1990.
16) Host-Madsen, A., and McCluskey, D.R., "On the Accuracy and Reliability of PIV Measurements", *Seventh International Symposium on Applications of Laser Anemometry to Fluid Mechanics*, Lisbon, Portugal, paper 26.4, 1994.
17) Huang, H., Dabiri, D., and Gharib, M., "On Errors of Digital Particle Image Velocimetry", *Measurement Science and Technology*, Volume 8, pp. 1427-1440, 1997.
18) Humphreys, W.M., Bartram, S.M., Parrott, T.L., and Jones, M.G., "Digital PIV Measurements of Acoustic Particle Displacements in a Normal Incidence Impedance Tube", *AIAA Paper 98-2611*, 1998.

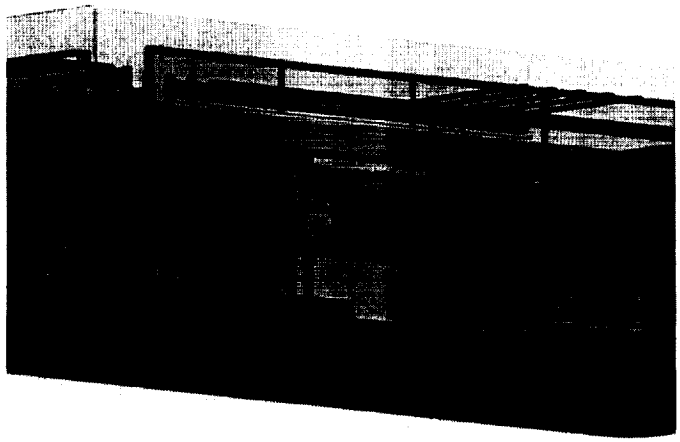

Figure 1. NASA Langley Subsonic Basic Research Tunnel.

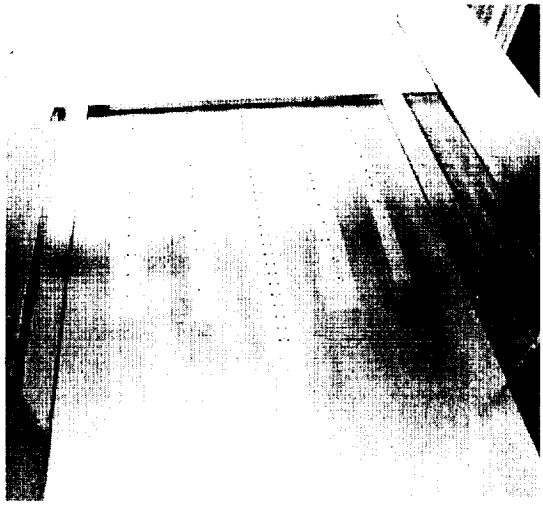

Figure 2. MSU Separated Flow Generator Model in SBRT.
Note Microphones, Pressure Taps, and DPIV Windows.

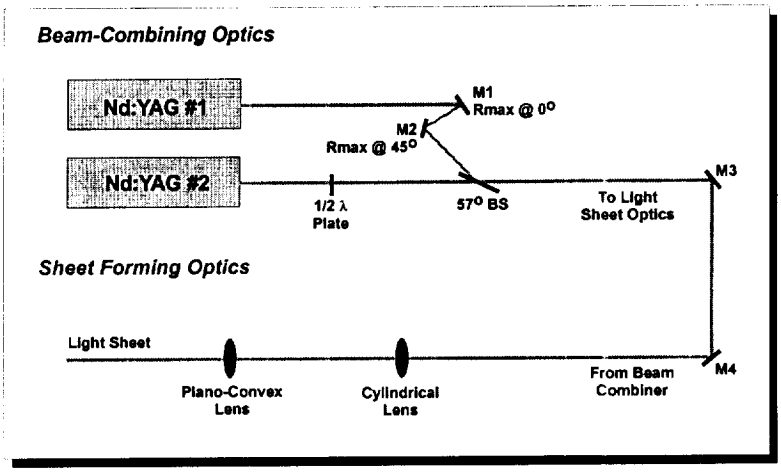

Figure 3. DPIV Laser Optics System.

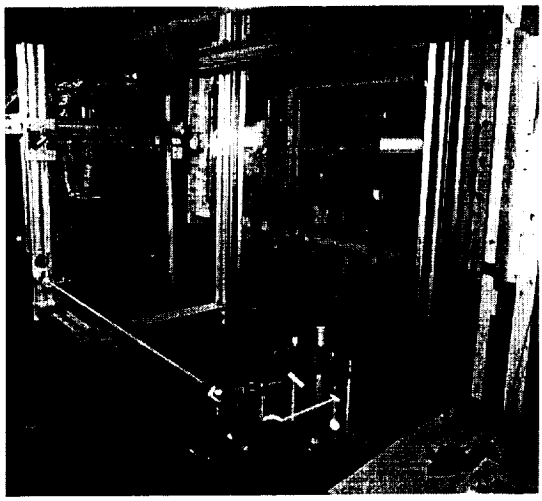

Figure 4. DPIV Laser Optics System in SBRT.

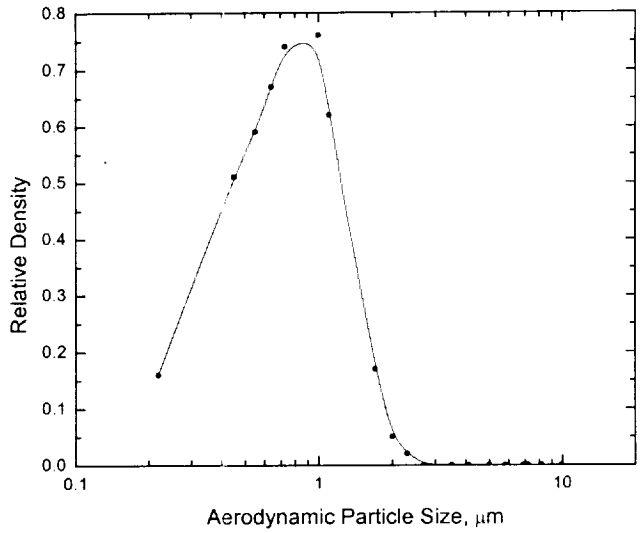

Figure 5. DEHS Nominal Particle Size Distribution.

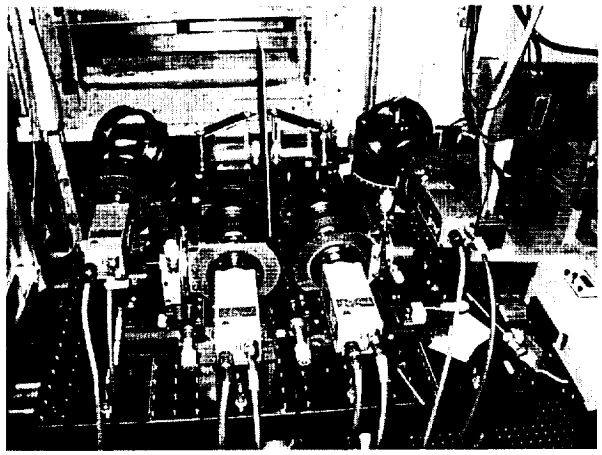

Figure 6. DPIV Recording System in SBRT.

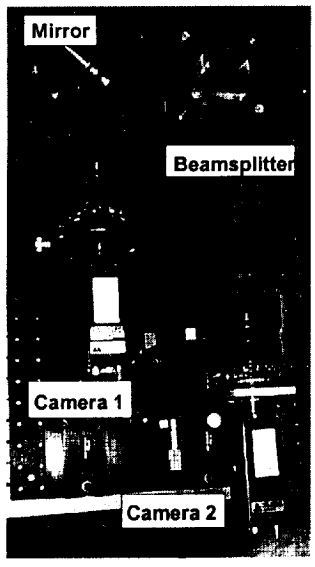

Figure 7. Recording System Receiver Configuration.

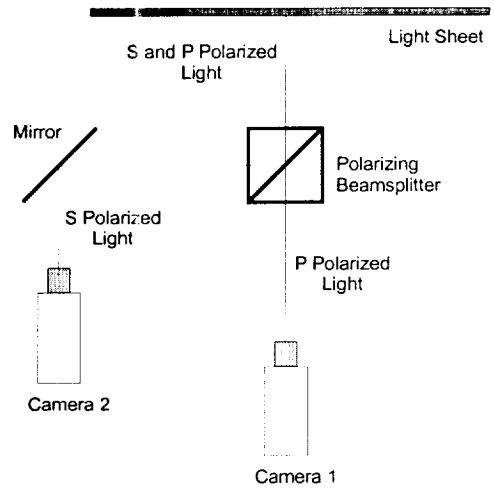

Figure 8. Polarization Separation Concept.

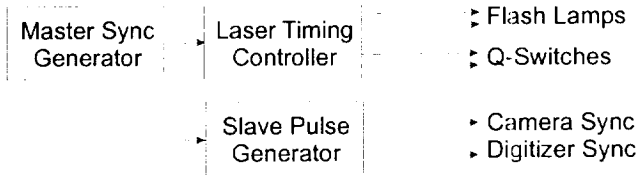

Figure 9. Laser / Camera Synchronization.

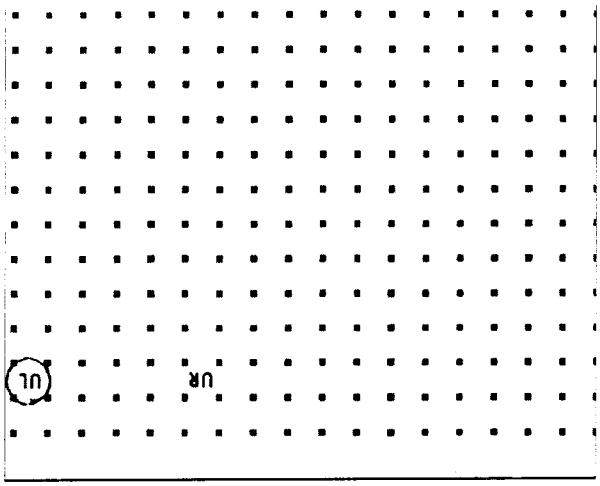

Figure 10. Pixel Alignment Dot Card.

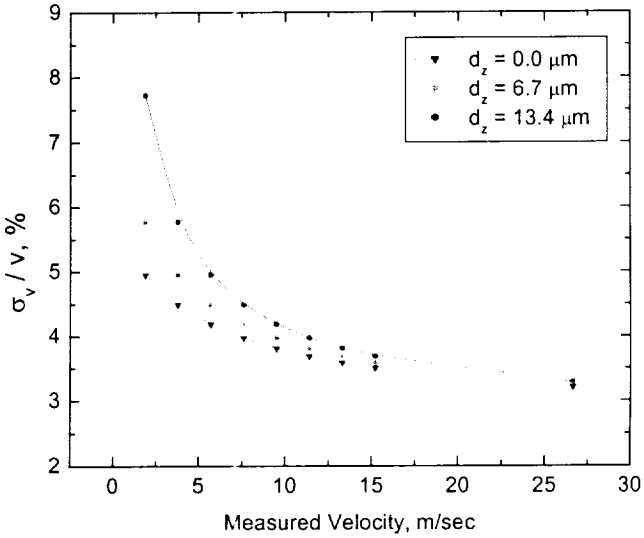

Figure 11. Velocity Uncertainty Estimates.

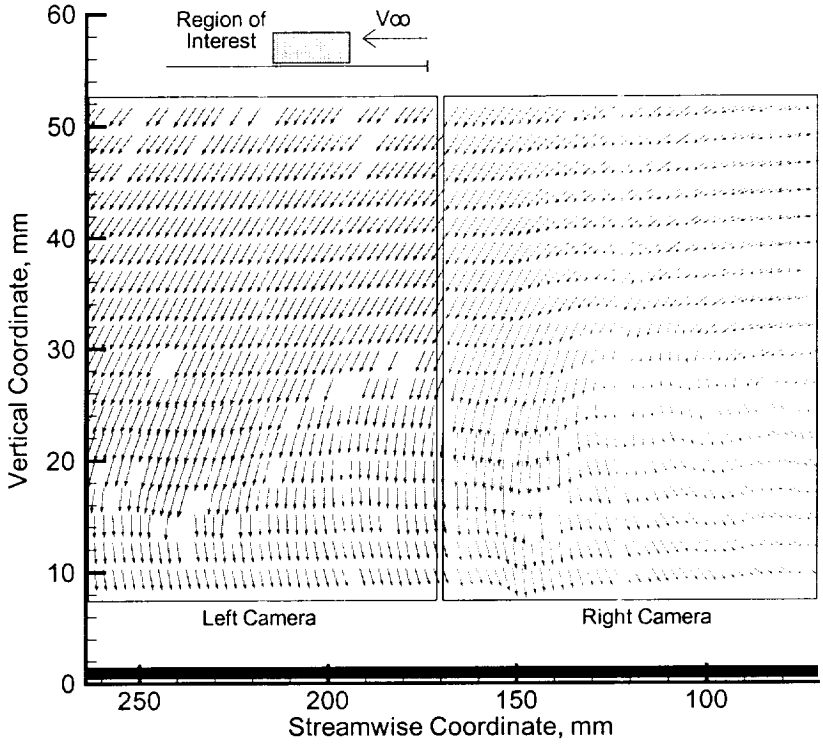

Figure 12. Representative Separated Flow Data Obtained Downstream of Splitter Plate Leading Edge Fence.